BIOCHEMICAL PHARMACOLOGY 77 (2009) 322–336

available at www.sciencedirect.com

ScienceDirect

journal homepage: www.elsevier.com/locate/biochempharm

Accumulation of artemisinin trioxane derivatives within neutral lipids of *Plasmodium falciparum* malaria parasites is endoperoxide-dependent

Carmony L. Hartwig [a], *Andrew S. Rosenthal* [b], *John D'Angelo* [b], *Carol E. Griffin* [a], *Gary H. Posner* [b], *Roland A. Cooper* [a,*]

[a] *Department of Biological Sciences,110 Mills Godwin Building/45th Street, Old Dominion University, Norfolk, VA 23529, United States*
[b] *Department of Chemistry and Malaria Research Institute, Johns Hopkins University, Baltimore, MD 21218, United States*

ARTICLE INFO

Article history:
Received 4 September 2008
Accepted 9 October 2008

Keywords:
Digestive vacuole
Heme
Reactive oxygen species
Lipid peroxidation
Free radicals

ABSTRACT

The antimalarial trioxanes, exemplified by the naturally occurring sesquiterpene lactone artemisinin and its semi-synthetic derivatives, contain an endoperoxide pharmacophore that lends tremendous potency against *Plasmodium* parasites. Despite decades of research, their mechanism of action remains unresolved. A leading model of anti-plasmodial activity hypothesizes that iron-mediated cleavage of the endoperoxide bridge generates cytotoxic drug metabolites capable of damaging cellular macromolecules. To probe the malarial targets of the endoperoxide drugs, we studied the distribution of fluorescent dansyl trioxane derivatives in living, intraerythrocytic-stage *Plasmodium falciparum* parasites using microscopic imaging. The fluorescent trioxanes rapidly accumulated in parasitized erythrocytes, localizing within digestive vacuole-associated neutral lipid bodies of trophozoites and schizonts, and surrounding the developing merozoite membranes. Artemisinin pre-treatment significantly reduced fluorescent labeling of neutral lipid bodies, while iron chelation increased non-specific cytoplasmic localization. To further explore the effects of endoperoxides on cellular lipids, we used an oxidation-sensitive BODIPY lipid probe to show the presence of artemisinin-induced peroxyl radicals in parasite membranes. Lipid extracts from artemisinin-exposed parasites contained increased amounts of free fatty acids and a novel cholesteryl ester. The cellular accumulation patterns and effects on lipids were entirely endoperoxide-dependent, as inactive dioxolane analogs lacking the endoperoxide moiety failed to label neutral lipid bodies or induce oxidative membrane damage. In the parasite digestive vacuole, neutral lipids closely associate with heme and promote hemozoin formation. We propose that the trioxane artemisinin and its derivatives are activated by heme-iron within the neutral lipid environment where they initiate oxidation reactions that damage parasite membranes.

1. Introduction

The control of malaria continues to be a global challenge due to the proliferation of multi-drug resistant *Plasmodium falciparum* parasites [1]. Derivatives of artemisinin (ART), a sesquiterpene lactone endoperoxide isolated from the herb *Artemisia annua*, are now widely used in the treatment of falciparum malaria. ART-based combination therapies (ACTs) have proven efficacious against multi-drug resistant parasites

* *Corresponding author*. Tel.: +1 757 683 4755; fax: +1 757 683 5283.
E-mail address: rcooper@odu.edu (R.A. Cooper).
0006-2952/$ – see front matter © 2008 Elsevier Inc. All rights reserved.
doi:10.1016/j.bcp.2008.10.015

and are now employed by more than 60 countries following World Health Organization recommendations [2]. Despite the extensive use of ACTs and development of new analogs, the specific molecular targets of the endoperoxides within *P. falciparum* remain poorly defined.

The potency of ART (Fig. 1(**1**)) depends on a unique 1,2,4-trioxane structure that contains an endoperoxide bridge; deoxy derivatives lacking a peroxidic bond have no significant antiparasitic activity [3]. Owing to the ability of ferrous iron to cleave organic peroxides into reactive free radicals [4], it was proposed that the endoperoxide bridge of ART is activated by cellular ferrous iron, forming free radical ART metabolites that damage critical cellular macromolecules [5,6]. Supporting the importance of iron-catalyzed activation are studies showing that iron chelation attenuates the potency of ART and related endoperoxides towards *Plasmodium* [7,8]. One source of cellular iron thought to catalyze peroxide opening is reduced heme (ferriprotoporphyrin IX), following which heme itself can become a target of alkylation [9]. From studies with a variety of antimalarial endoperoxides, there is growing evidence that heme alkylation is an important indicator of drug activity [10–14]. Heme-ART adducts are found in the spleen and urine of malaria-infected mice treated with therapeutically relevant doses of ART [15]. The parasite digestive vacuole (DV) is rich in heme due to proteolytic digestion of host hemoglobin [16], possibly explaining the high specific activity of ART against the parasite as opposed to normal mammalian cells [17]. Heme-catalyzed activation and alkylation is consistent with the detection of [^{14}C]-ART and [^{3}H]-dihydroART within the DV [18]. Additionally, one of the earliest physiological changes induced by the endoperoxides is disruption of the integrity of the DV membrane [19].

The precise molecular targets of antimalarial endoperoxides remain a topic of considerable debate [8,20,21]. Metabolites of ART can alkylate proteins in *P. falciparum*,

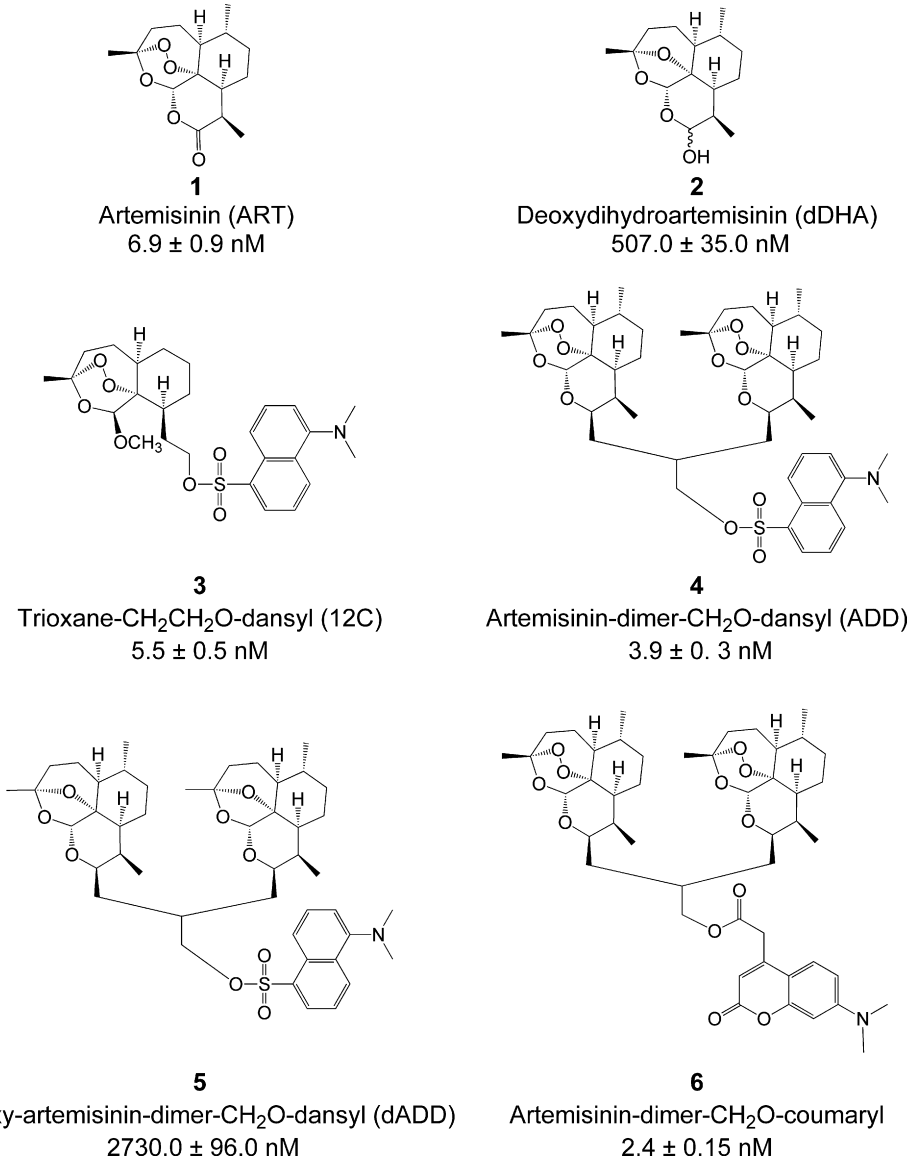

Fig. 1 – Structure of ART and related compounds used in this study. Also shown are in vitro IC_{50} values (mean ± SEM) for each compound, derived from three independent *P. falciparum* growth assays.

including a translationally controlled tumor protein homolog [22]. A recently proposed target of ART is the *P. falciparum* sarco/endoplasmic reticulum Ca^{2+}-ATPase (SERCA) homolog, PfATP6 [7]. The sesquiterpene lactone compound thapsigargin and ART competitively inhibit PfATP6 activity when expressed in *Xenopus* oocytes. However, the antimalarial contribution of specific protein binding by ART metabolites remains an open question. Field studies of PfATP6 have proven inconsistent; point mutations in the *pfatp6* gene were associated with reduced susceptibility to artmether in parasite isolates from French Guiana [23], but similar results have not been observed elsewhere.

Several lines of evidence support ART-induced oxidative stress as a plausible mechanism of action [20]. The in vitro potency of ART against *Plasmodium* is enhanced synergistically by the presence of increased oxygen tension or pro-oxidant drugs and inhibited by oxygen-radical scavengers [24]. Erythrocyte membrane models show that heme-ART binding leads to greatly enhanced heme-initiated oxidation and membrane damage, possibly through lipid peroxidation [25,26]. Exposure to ART or its derivatives results in the production of reactive oxygen species (ROS) in both yeast cells and mammalian tumor cells [27,28].

Confocal microscopy experiments with live *P. falciparum* demonstrated that fluorescent acridine ART derivatives localize in the parasite cytoplasm in an iron-dependent, covalent manner [7,8]. However, an ART-nitrobenzyldiazole conjugate, a fluorophore not quenched by heme, localized in the DV as well as the cytoplasm [8]. In these earlier studies, the effect of the endoperoxide bridge on accumulation was not directly investigated however. Here, we report on the chemical basis of localization and toxicity of the endoperoxides in *P. falciparum*. Using epifluorescence microscopy, we examined the intracellular distribution of novel fluorescent ART trioxane derivatives in living, parasite-infected erythrocytes (Fig. 1(**3**–**6**)). We compared a synthetic trioxane with several ART-based dimers and show that the endoperoxide pharmacophore underlies the specific accumulation of both structural types into neutral lipid bodies (NLB) of trophozoite- and schizont-stage parasites. A fluorescent ART probe, in which the endoperoxide bridge was replaced by an ether linkage, accumulated non-specifically in the parasite cytoplasm and showed only minimal activity against *P. falciparum*. We further show that the endoperoxide function was required to mediate changes in lipid composition and induce membrane peroxidation.

2. Materials and methods

2.1. Parasite culture

P. falciparum strain Dd2 was cultured in human AB^+ erythrocytes at 37 °C using RPMI 1640 (Mediatech, Herdon, VA) media supplemented with 0.5% Albumax I (Invitrogen, Carlsbad, CA), 0.25% $NaHCO_3$, and 0.01 mg/ml gentamicin (MP Biomedicals, Irvine, CA), under an atmosphere of 90% nitrogen, 5% oxygen, and 5% carbon dioxide. When required, parasite synchrony was maintained with 5% sorbitol treatment [29].

2.2. Synthesis of fluorescent compounds

2.2.1. Reagents

All chemicals, including ART and dihydroartemisinin were purchased from Sigma-Aldrich (St. Louis, MO) unless otherwise stated. Dansyl chloride and 7-dimethylaminocoumarin-4-acetic acid were purchased from Aldrich (St. Louis, MO). Solvents were supplied by Fisher Scientific (Pittsburgh, PA) or EMD Chemicals Inc. (La Jolla, CA) and were distilled to make anhydrous.

2.2.2. Synthesis of deoxydihydroartemisinin (dDHA; 2)

Dihydroartemisinin (0.5 g, 1.8 mmol) was dissolved in glacial acetic acid (20 ml) and stirred at room temperature under argon. When all the dihydroartemisinin had dissolved, zinc dust (0.89 g, 13 mmol), which was washed with 5% HCl (100 ml), ddH_2O (100 ml), EtOH (100 ml), and diethyl ether (100 ml), dried in vacuo, and stored under argon, was added. The mixture was then stirred for 5 h to completion. The mixture was filtered through a pad of Celite and washed with $CHCl_3$ (50 ml). The solution was then portioned between $CHCl_3$ (100 ml) and ddH_2O (100 ml). The layers were separated and the organic layer was washed with saturated sodium bicarbonate (3 × 100 ml) and brine, dried over Na_2SO_4, filtered and evaporated to a white solid. Purification by column chromatography (10% EtOAc/90% petroleum ether, then 100% EtOAc) gave the product dDHA as a white solid (0.24 g, 0.90 mmol, 50%) in a 2:1 mixture of isomers; mp = 134–136 °C.

2.2.3. Synthesis of trioxane-CH_2CH_2O-dansyl (12C; 3)

12C was synthesized according to published methods [30].

2.2.4. Synthesis of artemisinin-dimer-CH_2O-dansyl (ADD; 4)

Bis-trioxane primary alcohol was synthesized according to published protocols [31]. Dansyl chloride (134 mg, 0.495 mmol) was dissolved in dichloromethane (7 ml) with triethylamine (69 μl, 0.495 mmol) and stirred for 10 min. Bis-trioxane primary alcohol (100 mg, 0.165 mmol) was added and stirred at reflux for 18 h. The reaction was then allowed to cool and concentrated in vacuo. The crude product was purified by flash silica gel column chromatography (20% EtOAc/hexanes) to yield ADD as a bright yellow solid (101 mg, 0.120 mmol, 73%). mp = 110–112 °C; $[\alpha]_D^{22.5} + 40.62°$ ($c = 0.09$, $CHCl_3$). IR (CH_2Cl_2, film) 2938, 2875, 1713, 1575, 1454, 1376, 1356, 1176, 1105, 1053, 1008, 943, 881, 842, 790, 735, 632, 575; ^{1}H NMR (400 MHz, $CDCl_3$) δ 8.61 (br s, 1H), 8.33–8.27 (m, 2H), 7.58–7.52 (m, 2H), 7.20 (br s, 1H), 5.10 (s, 1H), 5.09 (s, 1H), 4.27–4.06 (m, 4H), 2.91 (s, 6H), 2.58–2.50 (m, 1H), 2.31–2.10 (m, 4H), 2.00–1.82 (m, 4H), 1.72–1.55 (m, 10H), 1.54–1.04 (m, 14H), 0.98–0.84 (m, 8H), 0.75–0.65 (m, 6H); ^{13}C NMR (100 MHz, $CDCl_3$) δ 131.63, 131.09, 130.55, 129.99, 129.86, 128.33, 123.31, 119.83, 115.29, 102.96, 102.40, 89.40, 88.90, 81.06, 80.88, 73.55, 73.01, 69.74, 52.28, 51.95, 45.48, 44.24, 43.88, 37.38, 37.33, 36.59, 34.46, 34.38, 33.82, 30.90, 30.41, 30.28, 29.59, 25.99, 25.90, 24.74, 24.67, 20.24, 20.06, 12.84, 12.30; HRMS (FAB-MS) *m/z* calculated for $C_{46}H_{65}NO_{11}S$ $[M+H]^+$ 840.4357, found 840.4352. To examine the possibility that the C-10 dansyl-linked fluorescent tag could be released by intraparasitic hydrolysis, ADD was dissolved in DMSO:D_2O at pH 7.4. After 0.5 h at 37 °C, the ADD dansyl sulfonate ester was approximately 20% hydrolyzed back into its parent primary alcohol.

2.2.5. *Synthesis of deoxy-dimer primary alcohol*

Zinc powder (192 mg, 2.94 mmol) was washed consecutively with 5% HCl (50 ml), ddH_2O (50 ml), EtOH (50 ml), diethyl ether (50 ml) and dried in vacuo. Bis-trioxane primary alcohol (120 mg, 0.198 mmol) was dissolved in glacial acetic acid (12 ml). The washed zinc was added to the acetic acid and stirred at room temperature for 2 h. The mixture was then filtered through Celite using $CHCl_3$. Filtrate was concentrated in vacuo to remove $CHCl_3$. The solid was then dissolved in dichloromethane (10 ml) and washed with saturated $NaHCO_3$ (2×10 ml). The organic layer was dried with $MgSO_4$, filtered, and concentrated in vacuo. The crude product was purified by flash silica gel column chromatography (40% EtOAc/hexanes) to yield deoxy-dimer primary alcohol as a white solid (93.0 mg, 0.162 mmol, 82%). mp = 84–85 °C; $[\alpha]_D^{23.2} - 110.76°$ (c = 0.080, $CHCl_3$). IR (CH_2Cl_2, film) 3524, 2950, 2875, 1456, 1384, 1266, 1208, 1178, 1141, 1099, 996, 925, 877, 735; ^{1}H NMR (400 MHz, $CDCl_3$) δ 5.27 (s, 1H), 5.26 (s, 1H), 4.28–4.17 (m, 2H), 3.77–3.57 (m, 2H), 2.46 (br s, 1H), 2.22–2.16 (m, 2H), 1.96–1.39 (m, 24H), 1.29–1.12 (m, 9H), 0.98–0.83 (m, 12H); ^{13}C NMR (100 MHz, $CDCl_3$) δ 107.14, 107.07, 97.23, 97.18, 82.45, 67.25, 65.09, 64.11, 45.36, 40.47, 35.72, 35.61, 34.57, 32.85, 32.63, 30.13, 30.00, 25.21, 23.73, 23.69, 22.19, 18.80, 12.16; HRMS (FAB-MS) m/z calculated for $C_{34}H_{54}O_7$ $[M+H]^+$ 575.3948, found 575.3943.

2.2.6. *Synthesis of deoxy-artemisinin-dimer-CH_2O-dansyl (dADD;* **5**)

Dansyl chloride (42 mg, 0.157 mmol) was dissolved in dichloromethane (2 ml) with triethylamine (22 μl, 0.157 mmol) and stirred for 10 min. Deoxy-dimer primary alcohol (30 mg, 0.052 mmol) was added and stirred at reflux for 18 h. The reaction was then allowed to cool and was concentrated in vacuo. The crude product was purified by flash silica gel column chromatography (20% EtOAc/hexanes) to yield dADD as a bright yellow solid (24.5 mg, 0.0303 mmol, 58%). mp = 100–110 °C; $[\alpha]_D^{21.1} - 86.45°$ (c = 0.485, $CHCl_3$). IR (CH_2Cl_2, film) 2953, 2872, 1574, 1459, 1384, 1358, 1266, 1206, 1176, 1142, 1100, 1010, 926, 877, 791, 736, 630; ^{1}H NMR (400 MHz, $CDCl_3$) δ 8.56–8.54 (d, J = 8.8 Hz, 1H), 8.31–8.29 (d, J = 8.8 Hz, 1H), 8.27–8.25 (m, 1H), 7.57–7.49 (m, 2H), 7.16–7.14 (d, J = 7.6 Hz, 1H), 5.05 (s, 1H), 4.89 (s, 1H), 4.31–4.08 (m, 2H), 4.05–3.96 (m, 2H), 2.87 (s, 6H), 2.10–1.94 (m, 3H), 1.85–1.75 (m, 4H), 1.69–1.00 (m, 22H), 0.97–0.83 (m, 12H), 0.74–0.72 (d, J = 7.6 Hz, 3H), 0.53–0.51 (d, J = 7.6 Hz, 3H); ^{13}C NMR (100 MHz, $CDCl_3$) δ 131.84, 130.98, 130.49, 130.13, 128.34, 123.00, 119.99, 115.21, 106.75, 106.65, 96.92, 96.87, 82.19, 82.08, 74.05, 65.76, 64.24, 45.46, 45.32, 45.29, 40.55, 40.35, 35.48, 34.55, 32.61, 31.91, 30.19, 29.76, 29.52, 24.98, 24.92, 23.71, 23.60, 22.16, 18.81, 12.30, 11.87; HRMS (FAB-MS) m/z calculated for $C_{46}H_{65}NO_9S$ $[M+H]^+$ 808.4458, found 808.4513.

2.2.7. *Synthesis of artemisinin-dimer-CH_2O-coumaryl (*6*)*

Bis-trioxane primary alcohol (98 mg, 0.16 mmol), 7-dimethylaminocoumarin-4-acetic acid (20 mg, 0.081 mmol) and 4-dimethylaminopyridine (10 mg, 0.08 mmol) were added to dichloromethane (7 ml) under argon. *N*,*N*′-dicyclohexylcarbodiimde (17 mg, 0.08 mmol) was added and the reaction was stirred at room temperature for 18 h. The orange solution was concentrated in vacuo. The crude product was purified by flash silica gel column chromatography (20–30% EtOAc/hexanes) to yield artemisinin-dimer-CH_2O-coumaryl as an amorphous pale yellow solid (28 mg, 0.033 mmol, 41%); $[\alpha]_D^{22.3} + 52°$ (c = 0.18, $CHCl_3$). IR (thin film) 3057, 2951, 2876, 1719, 1619, 1532, 1453, 1403, 1375, 1268, 1145, 1105, 1053, 1008, 735, 702 cm^{-1}; ^{1}H NMR (400 MHz, $CDCl_3$) δ 7.43–7.41 (d, J = 8.8 Hz, 1H), 6.64–6.61 (m, 1H), 6.51–6.50 (d, J = 2.0 Hz, 1H), 6.05 (s, 1H), 5.23 (s, 1H), 5.22 (s, 1H), 4.33–4.16 (m, 4H), 3.70 (s, 2H), 3.04 (s, 6H), 2.61–2.59 (m, 1H), 2.39–2.38 (m, 1H), 2.32–2.24 (m, 2H), 2.11–1.87 (m, 6H), 1.73–1.55 (m, 9H), 1.42–1.13 (m, 17H including singlets at 1.37 and 1.36), 0.95–0.85 (m, 9H), 0.78–0.76 (d, J = 7.2 Hz, 3H), 0.71–0.69 (d, J = 7.2 Hz, 3H); ^{13}C NMR (100 MHz, $CDCl_3$) δ 168.9, 161.6, 155.9, 152.7, 148.9, 125.6, 110.8, 109.2, 108.9, 103.2, 102.8, 98.4, 89.6, 88.9, 81.2, 81.1, 73.6, 70.5, 67.1, 52.3, 52.1, 44.4, 44.1, 40.2, 38.6, 37.5, 36.7, 36.6, 34.5, 34.4, 34.0, 30.1, 30.6, 30.4, 30.2, 26.1, 26.0, 24.8, 20.3, 20.1, 13.0, 12.5; HRMS (FAB) m/z calculated for $C_{47}H_{65}NO_{12}$ $[M+H]^+$ 836.4585, found 836.4578.

2.3. Drug susceptibility testing

Prior to testing, the structures of all new compounds were characterized by proton and ^{13}C NMR spectroscopy and by high-resolution mass spectrometry. All drugs were prepared as 10 mM stock solutions in DMSO or MeOH and stored at −30 °C. The in vitro susceptibility of *P. falciparum* to the various drugs was measured in a 72 h microplate growth assay using SYBR Green I (Molecular Probes) detection as described [32,33]. Mean half-maximal inhibitory concentrations (IC_{50} values) were derived by plotting percent growth inhibition against log drug concentration and fitting the response data to a variable slope sigmoidal curve-fit function using Prism 4.0c (GraphPad, San Diego, CA). IC_{50} values represent means ± standard error from at least three independent assays.

2.4. Fluorescence microscopy and image analysis

For live cell imaging, all culture or parasite samples were washed twice with PBS and mounted under coverslips with Slowfade Antifade Reagent (Invitrogen) in PBS. Isolated DVs were mounted in a similar fashion. Samples were viewed with 100× oil-immersion on an AX70 Olympus PROVIS U-CMAD3 epifluorescence microscope equipped with a 100W mercury bulb using U-MWU, U-MWB or U-MWG filter sets. Micrographic images were recorded using the Olympus DP70 camera system, and compiled and analyzed with Olympus DP Manager software and Photoshop CS v8.0 (Adobe Systems Incorporated, San Jose, CA).

2.5. Localization of 12C, ADD and dADD in *P. falciparum*

Mixed-stage *P. falciparum* cultures were exposed to 1 μM 12C or 1 μM ART for 10 min, or 500 nM ADD, 500 nM dADD, or 500 nM ADD plus 500 nM dADD for 30 min. Parasites were viewed directly or were first released from erythrocytes using 0.2% saponin. DVs from drug treated parasites were isolated according to published protocols [34,35].

2.6. Sub-cellular parasite labeling

Nile Red (ACROS Organics, Morris Plains, NJ) stock solution was prepared in MeOH at 1 mg/ml and stored at 4 °C.

MitoTracker Red 580, Lysosensor Green 189, ERTracker Green, DAPI nucleic acid stain and BODIPY 505/515 stock solutions were diluted in RPMI or PBS immediately prior to use and applied to live cultures according to the manufacturer's (Molecular Probes) suggested concentrations (see below). Prior to each experiment, fresh dilutions were made in RPMI or PBS. Trophozoite-stage parasite cultures (1% parasitemia) were incubated under one of the following conditions: 50 nM Lysosensor Green 189 for 1 min; 1 μM DAPI for 10 min; 1 μM ERTracker Green for 30 min, 500 nM MitoTracker Red 580 for 1 h, 500 nM BODIPY 505/515 for 30 min or 30 nM Nile Red for 10 min. Following incubation, cultures were exposed to 500 nM 12C for 10 min. With the exception of Lysosensor Green 189 and DAPI, cultures were first released from erythrocytes with 0.2% saponin prior to microscopic visualization to enhance fluorescence signal detection. For stage-specific accumulation of 12C and Nile Red, sorbitol-synchronized parasites, corresponding to six stages of intraerythrocytic growth, were subjected to the following treatments for 10 min prior to mounting for microscopy: drug-vehicle (0.01% MeOH), 30 nM Nile Red, 1.0 μM 12C or 12C plus Nile Red. Giemsa-stained thin smears were photographed under light microscopy at each time point to verify parasite stage. All stages, except for rings, were treated with 0.2% saponin for maximum fluorescence detection.

2.7. 12C competition experiments

Synchronized trophozoite-stage cultures were exposed to either 500 nM ART, 500 nM dDHA or drug-vehicle (0.01% MeOH) in pre-warmed complete media and incubated at 37 °C. After 10 min, the media was removed and replaced with fresh, pre-warmed complete media containing 500 nM 12C. Following 10 min incubation, parasites were washed, released with 0.2% saponin and processed for microscopy. The percentage of parasites showing detectable 12C NLB fluorescence was determined from 20 fields of view for each pre-treatment group (approximately 100 parasites per group). Mean volume of positive 12C signal per NLB for each pre-treatment group (consisting of 20–110 signals) was calculated from the intensity and area of signal in each frame using QuantityOne (Bio-Rad, Hercules, CA) software. Statistical analysis of pre-treatment effects on the percentage of 12C-positive parasites was evaluated with ANOVA and Tukey's post-hoc test ($p < 0.05$) for multiple comparisons. Pre-treatment effects on the mean volume of 12C signal for each pre-treatment group were evaluated using ANOVA ($p < 0.05$) and the Satterwhite approximation for degrees of freedom for unequal sub-sample comparisons [36]. Analyses were conducted with SPSS v16.0. Reciprocal experiments in terms of drug exposure order were conducted in the same fashion. Parasite cultures were first exposed to 500 nM 12C for 10 min, followed by 10 min ART post-treatment at 500 nM and 2 μM. All experiments were run in triplicate ($N = 3$).

2.8. Post-wash retention of ADD and dADD

Mixed-stage parasite cultures were treated with either 500 nM ADD or 500 nM dADD. Following 30 min drug exposure, cultures were washed in 37 °C complete media to remove drug, resuspended in drug-free complete media and incubated at 37 °C. At 10, 30, and 60 min post-wash, aliquots were removed from culture and parasites were released with 0.2% saponin and immediately processed for microscopy.

2.9. Thapsigargin and desferrioxamine inhibition experiments

Thapsigargin (Alexis, San Diego, CA), and desferrioxamine (Calbiochem, San Diego, CA) were resuspended in DMSO and ddH_2O, respectively, to a final concentration of 100 mM. Cultures of trophozoite-stage parasites were treated with 500 nM thapsigargin for 10 min or 100 μM desferrioxamine for 1 h, followed by either 500 nM 12C or 30 nM Nile Red staining for 10 min. Parasites were released from erythrocytes with 0.2% saponin prior to microscopic imaging.

2.10. Lipid peroxidation studies using BODIPY 581/591 C_{11}

The fluorescent BODIPY 581/591 C_{11} peroxidation-sensitive probe (Molecular Probes) was reconstituted to 40 μM in DMSO and stored under N_2. At ring, trophozoite and segmenter-stages, parasite cultures were exposed to 250 nM ART, 250 nM dDHA, 250 nM mefloquine (kindly provided by Dr. Thomas Wellems, National Institutes of Health, Bethesda, MD) or vehicle control (0.01% MeOH). After 3 h of drug exposure, cultures were labeled with 40 nM BODIPY 581/591 C_{11} and returned to 37 °C for an additional 30 min. Ring and segmenter-stage parasites occurred simultaneously in culture and were not saponin-released due to the difficulty pelleting freed ring-stage parasites, whereas trophozoite-stage parasites were released from erythrocytes using 0.2% saponin prior to visualization.

2.11. Thin-layer chromatographic analysis of lipids

Cultures of synchronous trophozoite-infected erythrocytes were treated with either 1 μM ART, 1 μM dDHA, 1 μM mefloquine or vehicle control (0.01% MeOH) for 5 h. Cultures were washed in PBS and erythrocytes were lysed with 0.2% saponin treatment. Cell pellets were extracted for total lipids with $CHCl_3$:MeOH:ddH_2O (8:4:3) according to established methods [37,38]. Control lipid extracts from uninfected erythrocytes, or uninfected erythrocytes treated with 1 μM ART, were prepared in a parallel fashion. Samples were dried under N_2 and resuspended in 50 ml of $CHCl_3$. Ten microlitres of each extract was applied to Silica Gel 60 thin layer chromatography (TLC) plates (Whatman, Florham Park, NJ), corresponding to $\sim 2.5 \times 10^8$ parasites, or $\sim 5 \times 10^9$ uninfected control erythrocytes. Non-polar lipid standards (Matreya, Pleasant Gap, PA) prepared in $CHCl_3$, at a final concentration of 25 mg/ml of each lipid species served as a reference for lipid extracts. Plates were visualized with 5% phosphomolybdic acid [39] (ACROS Organics) for overall lipid detection, or Liebermann-Burchard reagent [40] for specific sterol content, followed by heating at 110 °C for 5–10 min. Plates were photographed under transient illumination. Image background was adjusted using QuantityOne software (Bio-Rad).

3. Results

3.1. The fluorescent trioxane, 12C, accumulates in neutral lipid bodies

We used epifluorescence microscopy to study the intracellular distribution of fluorescent-tagged endoperoxides in living, *P. falciparum*-infected erythrocytes. The first endoperoxide we explored was compound 12C, a synthetic trioxane dansylate (Fig. 1(**2**)) whose synthesis and activity was described in an earlier study [30]. Growth-inhibition assays confirmed that 12C (IC_{50} = 5.5 nM) was equipotent to ART (IC_{50} = 6.9 nM) against the Dd2 strain of *P. falciparum*. ART and other endoperoxide drugs rapidly accumulate into *P. falciparum*-infected red blood cells [8,41] and are exceptionally fast-acting antimalarials [42]. Therapeutic plasma concentration of ART derivatives can achieve micromolar levels shortly after administration [43]. Therefore, to clearly detect fluorescence, we treated trophozoite-stage parasite cultures with 1 μM 12C for 10 min prior to microscopy. Fluorescence was observed as small, intensely bright spheres found in the parasite cytoplasm in proximity to the DV, which was distinguished by the presence of the dark hemozoin crystals (Fig. 2A; white arrowheads). Occasionally, faint, diffusive cytoplasmic fluorescence was noted in addition to the punctate labeling (not shown). No labeling was detected in uninfected red blood cells, demonstrating the specificity of drug accumulation by *P. falciparum*. No fluorescence was detected from control cultures treated with ART, showing that the 12C signal was not due to an inherent property of the endoperoxides to generate fluorescent metabolites. An earlier study showed labeling by a fluorescent ART-acridine conjugate in small membraneous structures of the erythrocyte cytoplasm, possibly corresponding to the parasite tubovesicular network [7]. Therefore, we released 12C-treated parasites from erythrocytes by saponin treatment prior to imaging (Fig. 2B). Parasite labeling was identical to that of infected erythrocytes, indicating that the fluorescence was contained within the parasite as opposed to the host erythrocyte cytoplasm. Finally, fluorescent labeling remained physically associated with the DV following their isolation by hypotonic lysis of the parasite membrane (Fig. 2C). Next, we examined the specificity of 12C labeling by comparing its intracellular distribution with that of fluorescent organellar and lipid probes. Merged images of trophozoite-infected erythrocytes and saponin-released trophozoites, counter-stained with probes specific for the DV, mitochondria, endoplasmic reticulum or nucleus, all show the distinct and separate localization of 12C (Fig. 3A). Depending on the orientation of the parasite, the images often suggested that the 12C-labeled spots resided within the DV compartment. However, further studies routinely showed they were located peripherally as opposed to internally. Parasites co-stained with 12C and the lipid probes BODIPY 505/515 or Nile Red showed overlapping, intense punctate fluorescence at the DV periphery, suggesting that the 12C-staining spots were lipid-rich.

From recent detailed imaging studies of the *Plasmodium* lipid environment, Nile Red has been shown to stain membrane structures of infected erythrocytes [37,44]. The most intensely stained regions were small cytoplasmic lipid droplets located adjacent to the DV exterior. These structures were identified as NLB, composed mostly of triacylglycerols (TAG). NLB are easily differentiated from parasite membranes as the spectral emission of Nile Red is based on the hydrophobicity of the lipid environment in which it is found [45]. Nile Red emits an intense yellow-green fluorescence when incorporated in neutral lipids, while polar lipids and phospholipids promote orange-red fluorescence (Fig. 3A). The clear overlap of 12C and Nile Red, shown in Fig. 3A, indicates that 12C fluorescence is specifically located in the NLB. We therefore studied the labeling patterns of 12C and Nile Red throughout the asexual stages of intraerythrocytic parasite growth. Parasite cultures exposed to 30 nM Nile Red for 10 min showed increasing numbers of NLB from the early trophozoite to schizont stages (Fig. 3B). When we applied 1 μM 12C to the parasites for 10 min, we observed a stage-specific labeling pattern that mimicked that of the Nile Red-stained NLB. Co-staining 12C-treated parasites with Nile Red resulted in overlap of the intense signal associated with the NLB, seen as a shift in the emission spectra compared to 12C or Nile Red alone. Labeling with either compound in ring-stage parasites resulted in faint fluorescence. In segmenter stages, 12C fluorescence was detected surrounding each merozoite in addition to the brighter signal of the NLB. Overlap of segmenter staining by 12C and Nile Red confirmed the affinity for the merozoites by both compounds.

3.2. ART specifically inhibits localization of 12C

Structurally diverse antimalarial endoperoxides vary in their cellular effects and affinity for different targets [13,19,46]. Therefore, we performed competition studies to determine if the NLB localization of 12C was also representative of ART. Parasite cultures were pre-treated for 10 min with either 500 nM ART or the inactive dioxolane, dDHA (Fig. 1(**2**)), then exposed to 500 nM 12C for an additional 10 min prior to imaging. Compared to the MeOH controls, no significant reduction of 12C fluorescence in NLB was detectable with dDHA pre-treatment (Fig. 4A). In contrast, when compared to the MeOH controls, ART pre-treatment resulted in a 77.1 ± 2.6% decrease in the number of parasites showing any detectable NLB fluorescence from 12C ($p < 0.01$) and a 74.6 ± 3.4% percent decrease compared to dDHA pre-treated controls ($p < 0.05$). Among parasites that contained fluorescing NLB in the ART pre-treatment group, the mean 12C signal volume was reduced by 72.4 ± 5.2% compared to control cells ($p < 0.01$; Fig. 4B). No significant difference was detected in mean NLB 12C signal volume between control cells pre-treated with MeOH or dDHA. The data suggest that ART and 12C share a similar ability to accumulate in NLB in an endoperoxide-dependent process. The finding that the inactive dDHA did not decrease the 12C signal suggests that ART and 12C may compete for binding or endoperoxide activation, as opposed to competing for uptake into the parasite. We next reversed the drug exposure protocol by pre-treating cultures with 500 nM 12C for 10 min and followed with equimolar or four-fold excess ART. In either case, no displacement of fluorescent labeling or decrease in signal intensity within NLB was observed (Fig. 4C). Taken together, these results indicate that labeling patterns were a result of activation of the 12C

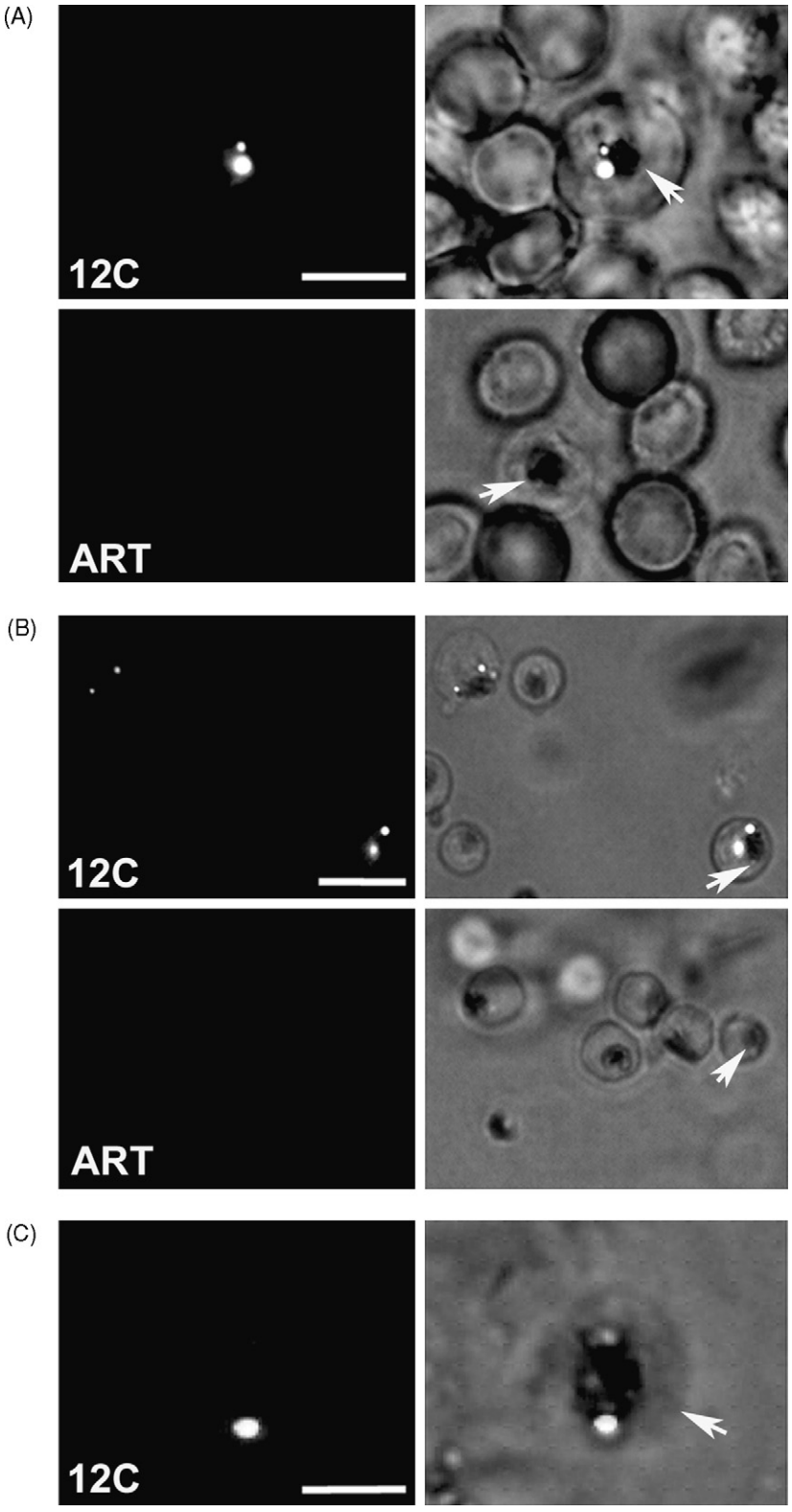

Fig. 2 – The fluorescent trioxane, 12C, accumulates in spherical structures closely associated with the parasite DV. Trophozoite-stage cultures were treated with 1.0 μM 12C (top rows) or ART (bottom rows) for 10 min prior to processing and microscopic visualization. (A) Trophozoite-infected erythrocytes. (B) Saponin-released trophozoites. (C) Isolated DV from a 12C-treated trophozoite. Left panels show fluorescence, while right panels show fluorescence merged with phase contrast. Parasites selectively accumulate 12C, which localizes within small (<1 μm) spheres adjacent to the parasite DV (white arrowheads). Scale bars represent 5 μm (A and B) or 2 μM (C).

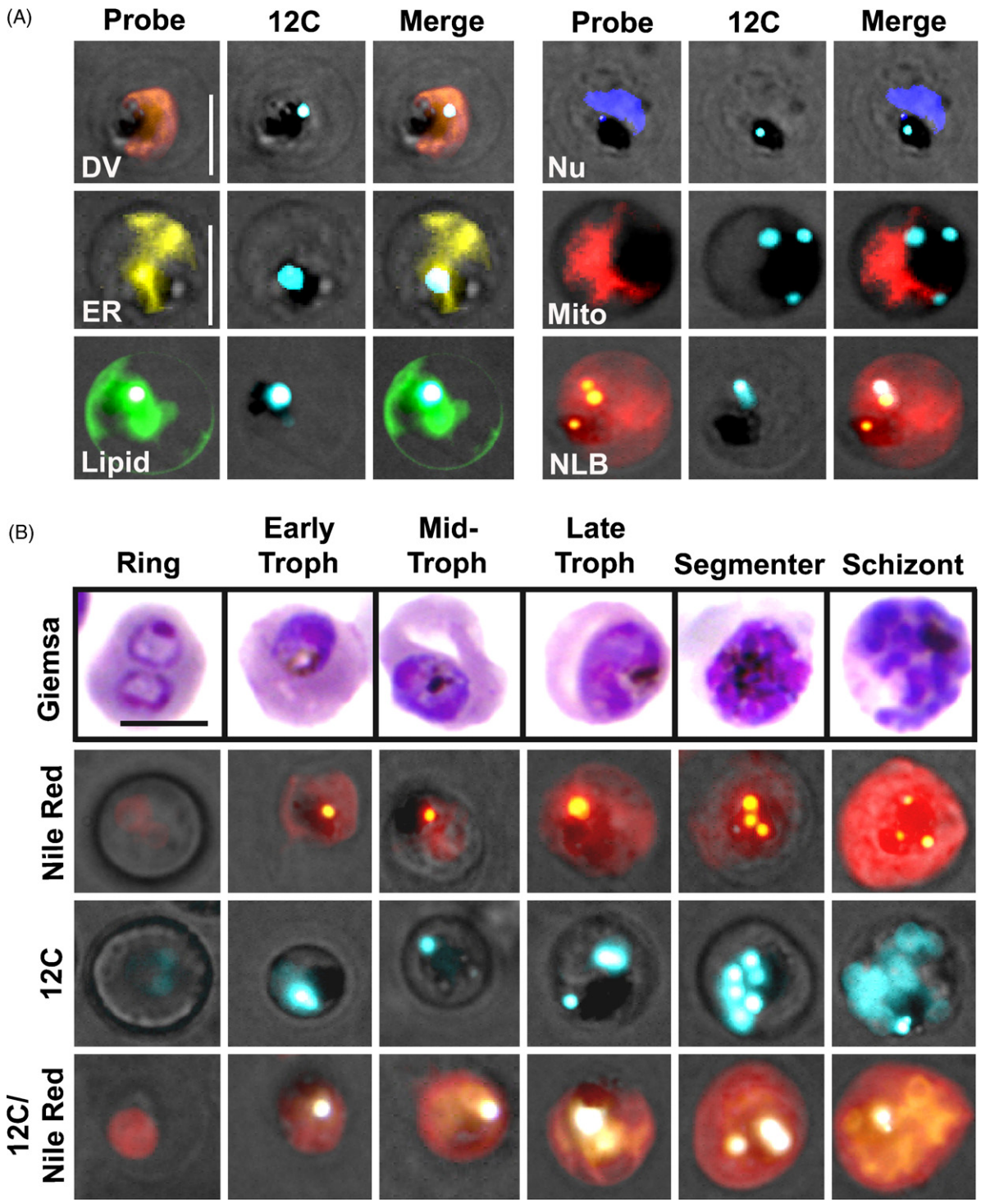

Fig. 3 – 12C labels parasite NLB and surrounds merozoite membranes. (A) Trophozoite-stage parasites were stained with the following probes: Lysosensor Green 189 for the DV, DAPI for the nucleus (Nu), ERTracker Green for the endoplasmic reticulum (ER), MitoTracker Red 580 for mitochondria (Mito), BODIPY 505/515 for neutral parasite lipids (Lipid) or Nile Red for detection of NLB. Following incubation with probes, cultures were exposed to 500 nM 12C for 10 min and processed for microscopic imaging. Columns represent probe fluorescence (Probe), 12C fluorescence (12C) or combined fluorescence of probe and 12C (Merge). Probes (except BODIPY 505/515 and Nile Red) were pseudo-colored to emphasize differential staining compared with 12C signal. Micrographs show merged fluorescence and phase contrast images of live trophozoite-infected erythrocytes (DV and Nu) or saponin-released trophozoites. (B) Merged images showing stage-specific staining of live cells with the lipid probe Nile Red (30 nM), 12C (1 μM) or both applied simultaneously. Nile Red exhibits an intense yellow-shifted fluorescence when incorporated into neutral lipids (second row). In addition to NLB of trophozoites (Troph) and schizonts, 12C fluorescence surrounds merozoites within segmented schizonts (third and fourth row, far right). Except for ring stages, parasites were released from erythrocytes by saponin treatment prior to imaging. Scale bars represent 5 μm.

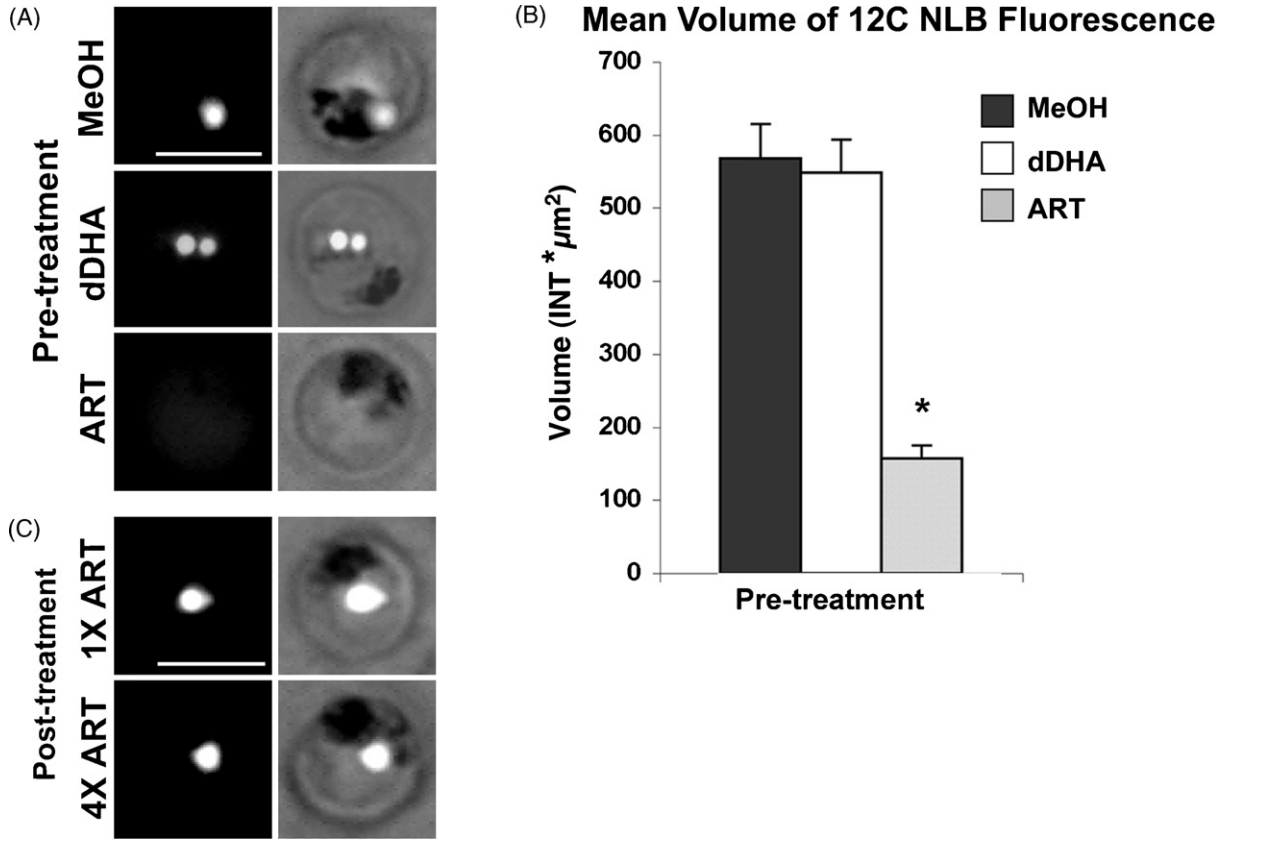

Fig. 4 – ART inhibits NLB accumulation of 12C but cannot displace pre-loaded 12C. (A) From top to bottom, panels show parasites pre-treated with MeOH (0.01%), 500 nM dDHA or ART prior to exposure to 500 nM 12C. Columns represent fluorescence (left) and fluorescence merged with phase contrast (right). Prior to imaging, parasites were released from erythrocytes by saponin treatment to increase accuracy of 12C signal intensity measurements. (B) Bar graph illustrating the mean volume of 12C fluorescence in NLB following pre-treatment with MeOH (dark grey), dDHA (white) or ART (light grey). Values represent mean 12C signal volume ± SEM, calculated from the average intensity (INT) and area (μm^2) of signal from labeled NLB. Means of 12C signal volume were derived from three independent experiments, where each experiment is an average of 20–110 individual intensity measurements (see Section 2). Asterisk denotes significant difference ($p < 0.01$) between mean volume of ART pre-treated samples and MeOH or dDHA controls. (C) Localization of 12C (500 nM) within NLB is not displaced by subsequent exposure to equimolar (top row) or excess (bottom row) amounts of ART. Columns represent same view as described in (A). Scale bars represent 5 μm.

endoperoxide moiety followed by alkylation of a target found within, or subsequently sequestered within, the NLB.

3.3. *Accumulation pattern of ART-derived dimers is endoperoxide-dependent*

Recently, a series of novel ART-derived trioxane dimers were shown to be highly potent and curative against murine malaria [47]. Based on this synthesis approach, we developed a matched pair of ART dimers conjugated to the same dansyl ester fluorophore used to construct 12C. These two dimers differed only in the presence of an endoperoxide or ether linkage within the ART framework, thus allowing the direct investigation of drug activation on cellular localization. Against the Dd2 strain of *P. falciparum*, in vitro drug assays showed that the trioxane ADD (Fig. 1(**4**)) was equipotent to ART and 700-fold more potent than the dioxolane derivative dADD, (Fig. 1(**5**)). Following treatment of cultures with 500 nM ADD for 30 min, bright fluorescence was detected in NLB in a pattern similar to 12C (Fig. 5A). In contrast, treatment with dADD resulted in uniform, cytoplasmic fluorescence with no evidence of specific organellar localization, including the NLB. When 500 nM ADD and dADD were administered to cultures simultaneously, the separate localization of each drug was clearly evident. Similar to what we observed for 12C in segmenter stages, ADD showed an affinity for labeling both the NLB and merozoites (Fig. 5B). As segmenters matured to the near release stage, NLB labeling became less distinct while the individual merozoite signal became more intense. The inactive dADD showed only weak, diffusive labeling of the segmenter stages, again demonstrating the necessity of the endoperoxide for specific drug localization. The cytoplasmic labeling and lack of anti-plasmodial activity by dADD illustrated important features of the dansyl tag: fluorescence was not attenuated when the drug was found in an aqueous compartment, nor did it impart potency or cause the probes to partition in lipid compartments. The starkly contrasting localization of the probes also argues that the visible

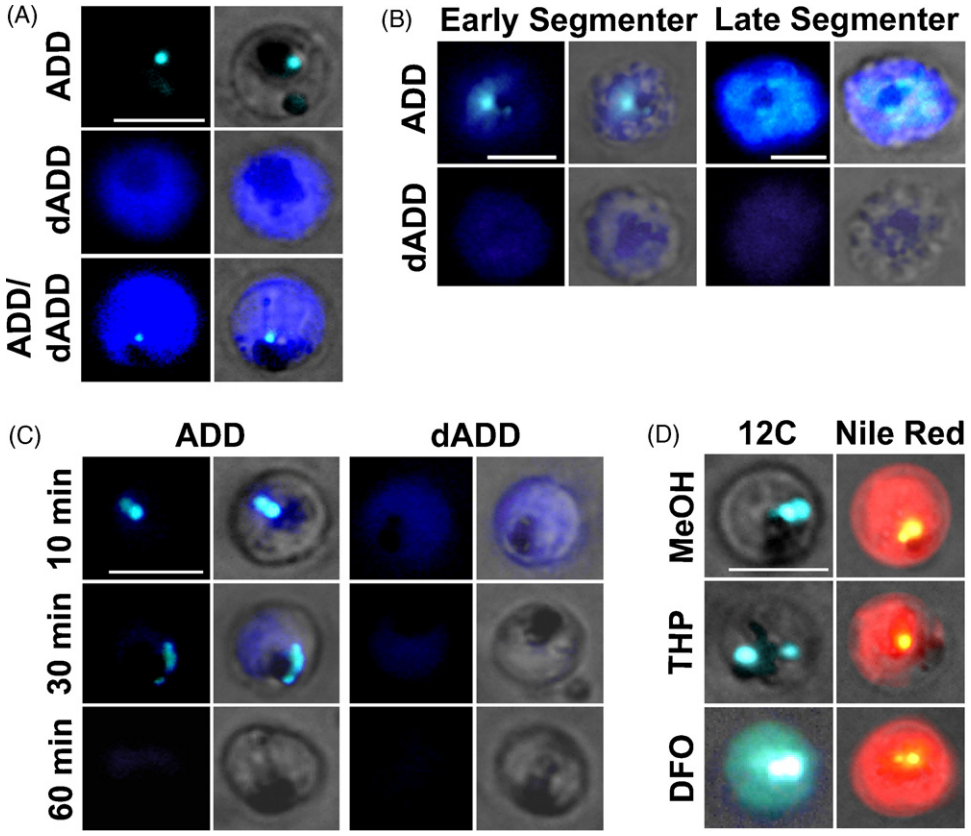

Fig. 5 – Localization of ART trioxane derivatives in NLB is endoperoxide-dependent. (A) Parasite cultures were treated with 500 nM ADD (top row), 500 nM dADD (middle row), or both ADD and dADD at 500 nM each, applied simultaneously (bottom row). Images show living, saponin-released trophozoites. Left panels show fluorescence, right panels are merged images. Pseudocoloring was used to emphasize contrast in the differential distribution of each drug. (B) Mixed cultures of early and late segmenter-stage parasites were treated with 500 nM ADD (top row) or 500 nM dADD (bottom row) for 30 min and imaged. For each stage, left panels show fluorescence, right panels are merged images. (C) Retention of ADD and dADD in parasites following wash-out of drug. Following a 30 min exposure to 500 nM of either drug, trophozoite-stage parasites were viewed 10 min (top row), 30 min (middle row), or 60 min (bottom row) post-wash. For each drug, left panels show fluorescence, right panels are merged images. (D) Effect of thapsigargin (THP) and desferrioxamine (DFO) on localization of 12C. From top to bottom, parasites were pre-treated for 10 min with MeOH or 500 nM THP, or for 1 h with 100 μM DFO, followed by exposure to 500 nM 12C (left column) or 30 nM Nile Red (right column) for 10 min. All images show merged fluorescence with phase contrast. Scale bars represent 5 μm.

fluorescence was not due to loss of the dansyl probe through hydrolysis of the C-10 linkage.

Since intracellular labeling patterns by the ART dimers were endoperoxide-dependent, we tested the hypothesis that ADD formed covalent adducts with target molecules, while predicting that dADD was unlikely to bind covalently. We treated parasites with 500 nM ADD or dADD for 30 min, removed drug from the cultures with fresh media changes and imaged at various time points post-wash (Fig. 5C). At 10 min post-wash, ADD-treated parasites retained bright fluorescence in the NLB, but the signal gradually diminished by 60 min post-wash. In contrast, washing of dADD-treated parasites resulted in a rapid dissipation of the cytoplasmic fluorescence, which was barely detectable after 30 min. These findings suggested that ADD binds tightly to its target(s) within the NLB, but turnover of this binding site occurred, as signal was gradually lost after 60 min. In keeping with its low potency, the rapid disappearance of dADD fluorescence suggests that the drug does not posses strong binding affinity for specific molecular targets.

3.4. *Effect of ART inhibitors thapsigargin and desferrioxamine on 12C labeling*

In *P. falciparum*, ART was shown to inhibit cytoplasmic labeling by a fluorescent thapsigargin analog, presumably by competitively binding the SERCA analog, PfATP6 [7]. Therefore, we used thapsigargin pre-treatment to study the possible involvement of PfATP6 in the intracellular distribution pattern of 12C. We found that pre-treatment with 500 nM thapsigargin for 10 min had no effect on equimolar 12C localization in the NLB (Fig. 5D). Staining of thapsigargin-treated parasites with Nile Red demonstrated that NLB formation was unaffected by thapsigargin pre-treatment. These results rule out PfATP6 involvement in the localization of 12C to NLB.

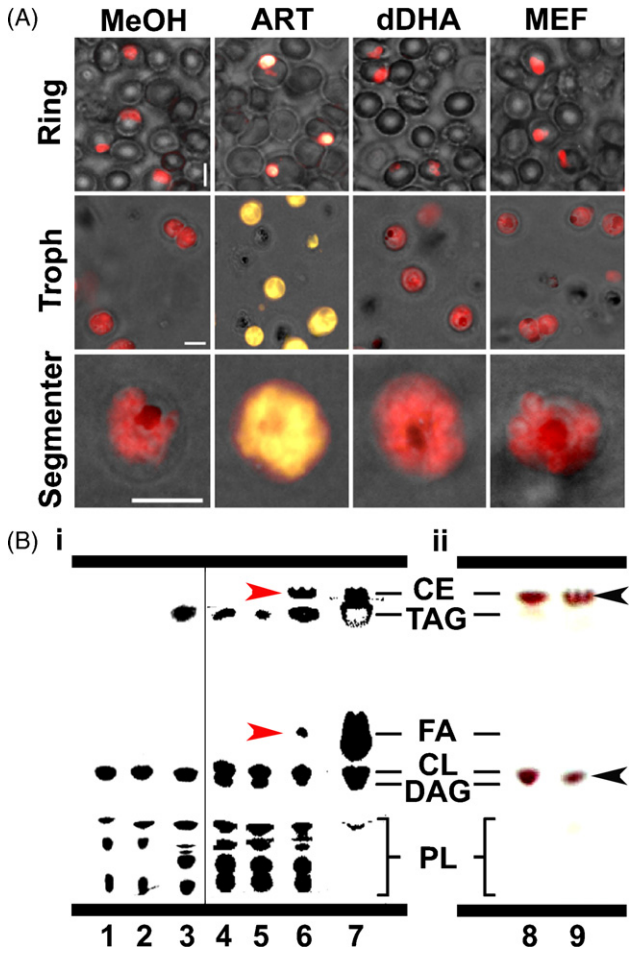

Fig. 6 – Exposure to ART results in formation of peroxyl radicals and alters parasite lipid composition. (A) Oxidation of BODIPY 581/591 C_{11} in ring, trophozoite (Troph) and segmenter-infected cultures after 3.5 h exposure to MeOH (0.01%), or 250 nM ART, dDHA or mefloquine (MEF). All panels show fluorescence merged with phase contrast. Only ART produces an emission shift in BODIPY 581/591 C_{11}, indicating the presence of peroxyl radicals in the parasite lipid environment is endoperoxide-dependent. Scale bars represent 5 μm. (B) Exposure to ART results in modification of parasite lipids. Parasites were exposed to 1 μM of each drug for 5 h prior to lipid extraction. Erythrocyte and parasitized erythrocyte lipid extracts were separated by TLC as described in Section 2. (i) Total lipid analysis of uninfected erythrocytes (lane 1); uninfected erythrocytes incubated with ART (lane 2); parasitized erythrocytes exposed to MEF (lane 3), MeOH (lane 4), dDHA (lane 5) or ART (lane 6); lipid migration standard containing cholesteryl ester (CE), triacylglycerol (TAG), fatty acids (FA), cholesterol (CL), diacylglycerol (DAG), phospholipids (PL) (lane 7). ART treatment (lane 6) results in an increase in FA content (bottom red arrowhead), and a lipid species not observed in control treatments, with a similar mobility to the CE standard (top red arrowhead). (ii) Plates were derivatized with the Liebermann-Burchard reagent for detection of CL and CE. In both the lipid standard (lane 8) and in the ART-treated parasite lipid extracts (lane 9), derivatization results in a brown-violet CE band (top black arrowhead) and a violet CL band (bottom black arrowhead). In (i) and (ii), solvent front was run to 0.5 cm from top of the plate, and background was eliminated to enhance contrast of bands. (For interpretation of the references to color in this figure legend, the reader is referred to the web version of the article.)

Desferrioxamine, a chelator of free ferric iron, antagonizes the potency of ART and abolishes the irreversible binding of fluorescent ART derivatives in *P. falciparum*-infected erythrocytes [8,48]. We therefore examined the effect of desferrioxamine on NLB labeling by 12C in trophozoites. In addition to the bright labeling of NLB, pre-treatment with 100 μM desferrioxamine for 1 h followed by 500 nM 12C resulted in substantial cytoplasmic fluorescence (Fig. 5D). Staining with Nile Red demonstrated that desferrioxamine pre-treatment had no observable effect on the presence of NLB. The diffusive cytosolic 12C staining resulting from desferrioxamine pre-treatment resembled that of the inactive dimer, dADD (Fig. 5A), suggesting that some of the 12C taken up by parasites was not subjected to endoperoxide activation. The continued labeling of NLB suggested that despite chelating with desferrioxamine additional sources of iron remained available to activate a portion of the 12C. These findings nonetheless demonstrate that iron-catalyzed activation of endoperoxides is likely an important step in the accumulation of 12C within NLB.

3.5. *Formation of reactive oxygen species in parasite membranes is endoperoxide-dependent*

ART has been shown to cause oxidative damage to red blood cell and yeast membranes through formation of iron-catalyzed free radicals and formation of downstream ROS [25,26,28]. Given the selective accumulation of 12C and ADD in neutral lipids, we used BODIPY 581/591 C_{11} to test for the presence of ROS in the parasite membrane system following exposure to ART. A fluorescent fatty acid, BODIPY 581/591 C_{11} is efficiently incorporated into cellular membranes and is oxidized by various radicals, causing the normal red fluorescence to shift to green [49]. Parasite cultures were treated with various drugs at 250 nM for 3 h and co-incubated with BODIPY 581/591 C_{11} for 30 min prior to imaging under epifluorescence microscopy (Fig. 6A). Control cells showed strong incorporation of the lipid probe at all stages, and retention of the red fluorescence indicated that no auto-oxidation occurred during processing. In contrast, BODIPY 581/591 C_{11} rapidly oxidized in ring, trophozoite and segmenter-stage parasites treated with ART, consistent with reports of ART potency against all asexual blood stages of the parasite [17]. Incorporation of the probe into membrane appeared non-specific, and all labeled areas showed extensive oxidation following ART treatment. The yellow-green probe color was less intense in the ring-stage parasites compared to later stages, consistent with the diminished quantity of 12C labeling of rings shown in Fig. 3B. Cultures treated with inactive dDHA showed red fluorescence identical to controls, indicating the probe had not been oxidized (Fig. 6A). We also treated BODIPY 581/591 C_{11} labeled cells with 250 nM mefloquine, a potent quinoline alcohol that

binds heme with high affinity [50]. Treatment with mefloquine resulted in no observable shift in the emission spectra of the probe. These results confirmed that the endoperoxide group of ART was required to induce oxidative processes in the membranes of *P. falciparum*. We observed that the oxidation of BODIPY 581/591 C_{11} was minimal if cells were labeled promptly after ART exposure (data not shown). Rather, the probe emission shift began to peak at least 3 h post-ART exposure, suggesting that oxidation may be due to downstream ROS species formed in chain reactions within the membrane.

3.6. ART exposure alters composition of lipid species in parasitized erythrocytes

We used TLC analysis to determine if ART exposure affected the lipid content of *P. falciparum*. Lipid extracts, from saponin-lysed, infected and uninfected erythrocytes exposed to 5 h drug-treatment, were separated on silica plates in a two-stage solvent system that resolves both phospholipids and neutral lipids (Fig. 6B (i)) [37]. Exposure to 1 μM ART had no observable effect on the lipid composition of uninfected erythrocytes (Fig. 6B (i), lanes 1–2). Compared to uninfected erythrocytes, infected cells were enriched in phospholipids and TAG (lanes 3–6) as reported elsewhere [37,44]. Drug-vehicle, dDHA and mefloquine had no effect on any of the lipid species resolved from trophozoite-infected cells (lanes 3–5). However, treatment of infected erythrocytes with 1 μM ART resulted in the appearance of two additional bands compared to controls (lane 6). The smaller band co-migrated with the fatty acid (FA) standard, while a larger band co-migrated with the cholesterol oleate (a cholesteryl ester; CE) standard. Because *P. falciparum* is not known to synthesize CE, we sprayed plates with Liebermann-Burchard reagent to verify the presence of sterols (Fig. 6B (ii)) [40]. The additional band from the ART-treated parasites both co-migrated and stained the same brown-violet color as the CE standard, but distinct from the violet-staining cholesterol (CL), strongly suggesting the presence of a CE. The presence of the FA and CE bands was both parasite and endoperoxide-dependent. The identification of the larger band as a possible CE not normally found in *P. falciparum* suggests these lipids resulted from free radical processes initiated by parasite-activated ART.

4. Discussion

We investigated the cellular targets of antimalarial endoperoxides using novel fluorescent-tagged ART trioxane derivatives in conjunction with microscopic imaging of living *P. falciparum* parasites. Supporting the hypothesis of ART bioactivation, we show that the endoperoxide pharmacophore underlies the accumulation of drug metabolites in parasite neutral lipid compartments and their ability to initiate oxidative membrane damage. Our probes were based on a synthetic tricyclic trioxane (12C) or semi-synthetic ART-derived dimers (ADD and dADD) [30,31], both conjugated with a dansyl fluorophore. Both 12C and ADD were of similar potency (IC_{50} values from 3.9–5.5 nM) to ART (6.9 nM) against the Dd2 strain of *P. falciparum*. The inactive dioxolane dimer, dADD (IC_{50} = 2730 nM) was structurally identical to ADD, except that dADD contained ether linkages instead of endoperoxide bridges and was therefore not susceptible to iron-catalyzed activation.

P. falciparum-infected erythrocytes rapidly accumulated both pharmacologically active and inactive fluorescent probes. Beginning with early trophozoite stages, 12C and ADD labeling closely overlapped the characteristic bright yellow-orange staining of NLB by Nile Red [37,44]. NLB are small lipid droplets composed primarily of TAG, diacylglycerol or sterol esters and appear ubiquitously in eukaryotic cells [51,52]. In *Plasmodium*, they are likely reassembled from phospholipids derived from membrane-bound, hemoglobin-filled vesicles that are ingested into the DV. NLB may provide energy and precursors for membrane biogenesis in the maturing parasite [53]. In the DV, neutral lipid nanospheres are believed to concentrate the lipophilic free heme, while promoting heme crystallization at the lipid-cytosol interface [38]. This places neutral lipids in the same environment where heme-mediated ART activation is predicted to take place.

The immediate, striking disparity in NLB localization of 12C or ADD versus dADD in the parasite cytoplasm provides strong evidence that endoperoxide activation and formation of alkylating metabolites were necessary precursors to neutral lipid labeling. The inability of ART to displace NLB labeling and the slow washout of ADD compared to dADD supports the formation of covalently bound probe adducts. The dADD probe, lacking the endoperoxide group, did not form tightly bound metabolites, as evidenced by the rapid washout of fluorescence from the cell. One possible target of alkylation is TAG, although lipid-ART adducts have yet to be documented. We thus favor heme as a more plausible target, as discussed below.

Although 12C fluorescence was faint in ring-stage parasites, our results demonstrated endoperoxide-induced lipid peroxidation in all parasite stages. This argues that rings contain sufficient ferrous iron available for drug activation, consistent with recent studies showing that rings more actively ingest hemoglobin than previously believed [54,55]. As parasites mature, TAG-rich NLB accumulate around the DV periphery [44]. Prior to parasite release, NLB begin to disperse and TAG is found surrounding the enclosed merozoites, resulting in a ''bunch of grapes'' staining pattern with Nile Red [44]. The close overlap of Nile Red and 12C or ADD in trophozoite and schizont NLB, as well as dispersed around growing merozoites, suggests that the drug metabolites or adducts have a strong affinity for the highly lipophilic TAG-rich compartments. Our results indicate that all asexual parasite stages should be susceptible to endoperoxides. However, literature reports of stage susceptibility to ART are variable and contradictory [17], thus more studies are required to resolve these discrepancies.

The cellular distribution of 12C and ADD sharply contrasts with earlier reports of cytoplasmic and DV localization of fluorescent acridine- or nitrobenzyldiazole-conjugated endoperoxides [7,8]. Physicochemical differences in the endoperoxide framework and the 2,6-dansyl fluorophore may account for these observations. The substantially more polar acridine and nitrobenzyldiazole tags (Posner, unpublished data) could bias probe localization away from hydrophobic compart-

ments. The inhibition of 12C NLB fluorescence by ART showed that the specific localization of the dansyl-tagged probes was representative of other trioxane derivatives, but does not rule out other ART targets. We also tested a coumaryl-conjugated ART dimer (Fig. 1 (**6**)), and found similar labeling of the NLB (data not shown). Interestingly, we did not observe DV localization of our probes, suggesting that 12C and ADD fluorescence may have been quenched by hemozoin and/or acidic pH, similar to the acridine trioxane probes [7,8]. Alternatively, the immediate activation of 12C and ADD may have precluded DV visualization.

Chelating iron attenuates the cytotoxic effects of ART in *Plasmodium*, *Saccharomyces* and cancer cells [8,28,48,56]. Here, desferrioxamine treatment did not inhibit uptake of 12C, but a portion of the fluorescence remained in the parasite cytoplasm, similar to inactive dADD labeling. Desferrioxamine may have removed free iron available for endoperoxide activation and the resulting cytoplasmic fluorescence represented intact 12C. Since desferrioxamine selectively binds free ferric iron [8], ferrous heme in the DV would remain available for activation, and may correspond to the 12C observed in the NLB. The effects of chelation are not easily explained because endoperoxides are relatively inert in the presence of ferric iron [57], leading to the proposal that desferrioxamine might alter the intracellular ferric and ferrous iron equilibrium [8].

The sesquiterpene lactone, thapsigargin, is a specific inhibitor of mammalian SERCA [58] and has been shown to compete with ART for binding of the *P. falciparum* ortholog, PfATP6, when expressed in *Xenopus* oocytes. In *P. falciparum*, thapsigargin blocked the cytoplasmic labeling of an ART-acridine probe [7]. These observations led to the proposal that PfATP6 is the primary target of ART alkylation and inhibition. In direct contrast, thapsigargin showed no ability to reduce the accumulation of 12C into NLB, indicating that interactions with PfATP6 are unlikely to account for the labeling patterns we observed. In agreement with our observations, recent isobole studies have failed to reproduce the proposed antagonistic relationship between ART and thapsigargin [19].

Endoperoxide-induced oxidative stress has been proposed as a mechanism of action of ART [20,24,28]. Earlier studies showed that ART greatly enhances heme-catalyzed lipid peroxidation and oxidative protein damage in erythrocyte membrane preparations [25,26]. Our results with the oxidation-sensitive probe, BODIPY 581/591 C_{11}, demonstrated the formation of ART-induced peroxyl radicals in parasite membranes during intraerythrocytic, asexual stages. The generation of ROS by ART was endoperoxide-specific, as experiments with dDHA produced no observable shift in the emission spectra of the probe. We found that BODIPY 581/591 C_{11} peroxidation was evident after 3 h exposure to ART, which also corresponded to the longer incubation time required to detect CE and free FA. This suggests that accumulation of endoperoxide metabolites in neutral lipids may be necessary to initiate peroxyl radical formation among unsaturated lipids, whereas the detrimental effects of chain-propagating reactions on parasite membranes are only evident following longer exposure times (>3 h). Alternatively, there may be a time lag as the antioxidant defenses of the parasite are exhausted.

We found that ART caused an increase in the amount of free FA in the parasite. Normally, large quantities of free FA are released in conjunction with TAG degradation in late schizogony, possibly in association with erythrocyte rupture [44]. The localization of 12C and ADD metabolites in TAG-rich compartments may induce premature breakdown of TAG into free FA. Unsaturated FA are readily oxidized in the cell, and exposure to oxidized polyunsaturated FA can markedly inhibit *Plasmodium* growth in vivo and in vitro [59]. Further studies are needed to elucidate the structure(s) of the ART-induced FA to determine their possible role in drug potency.

A surprising result was the appearance of an ART-induced CE in parasite lipid extracts. CL esterification activity has not been detected in *P. falciparum*, although the genome contains lecithin-cholesterol acyltransferase (LCAT) and acyl CoA:diacylglycerol transferase (DGAT) genes, both with peak transcript expression levels in schizont stages [51,60,61]. CL is a neutral lipid that is highly prone to free radical oxidation to form various oxysterol derivatives, particularly in the presence of polyunsaturated FA peroxides [62,63]. Oxysterols are considered better substrates for enzymatic esterification than CL itself [64], thus an oxysterol could become a substrate for esterification activity by *P. falciparum* LCAT or DGAT. *P. falciparum* incorporates host CL into it own membranes, where it is essential for the maintenance of intracellular infection [44,61,65]. As CL is relatively scarce in parasite membrane, esterification of this vital cellular component may be deleterious to parasite survival. Structural verification of the putative CE will facilitate an understanding of the biosynthetic pathway induced by ART.

In summary, the endoperoxide probes, 12C and ADD, despite having markedly different chemical structures, specifically labeled neutral lipid compartments. Moreover, because ART inhibited NLB labeling, our study agrees with previous results that indicate a common pathway of activation and alkylation for structurally diverse endoperoxides in *P. falciparum* [8]. We propose a model where ART trioxane derivatives rapidly accumulate in the DV and are activated by neutral lipid-associated heme [38]. The reactive metabolites alkylate heme, forming highly lipophilic adducts that remain trapped in the neutral lipids that are sequestered in NLB on the DV exterior. Heme adducts of various endoperoxides are well described from in vitro and in vivo studies [10–15] and are unlikely to be incorporated into hemozoin [14]. In the NLB, heme adducts may initiate lipid peroxidation and generation of ROS due to the abundance of unsaturated FA [20]. Heme induces substantial oxidative stress on the lipids of *P. falciparum*. Large amounts of hydroxy fatty acids are generated in the parasite by heme-catalyzed peroxidation of phospholipids [66]. ART alkylation further enhances the oxidative capacity of heme to damage lipid membranes [26]. These observations may explain DV membrane damage as one of the earliest effects of ART in *P. falciparum* [19]. The quantitative contribution of oxidative stress to the potency of the endoperoxides remains to be established. However, the generation of ROS by ART derivatives in a variety of eukaryotic cell types [27,28,67], in juvenile schistosomes [68], and in *P. falciparum*, is clearly associated with cytotoxicity. Overall, this study provides evidence that the interaction of endoperoxides with neutral lipids may be an important component in their mechanism of action against malaria parasites.

Acknowledgments

We thank Jonathan M. Hoke and Paul Roepe for technical assistance, and Leanne Tilley and John Pisciotta for helpful discussions. R.A.C. and C.L.H. were supported by National Institutes of Health Grant AI055601, and in part by the Jeffress Memorial Foundation Grant J-725. G.H.P., A.S.R., and J.G.D. were supported by National Institutes of Health Grant AI34885.

REFERENCES

[1] Hyde JE. Drug-resistant malaria – an insight. FEBS J 2007;274:4688–98.
[2] Plowe CV, Roper C, Barnwell JW, Happi CT, Joshi HH, Mbacham W, et al. World Antimalarial Resistance Network (WARN) III: molecular markers for drug resistant malaria. Malar J 2007;6:121–30.
[3] Jefford CW, Vicente MGH, Jacquier Y, Favarger F, Mareda J, Millasson-Schmidt P, et al. The deoxygenation and isomerization of artemisinin and artemether and their relevance to antimalarial action. Helvetica Chim Acta 1996;79:1475–87.
[4] Gutteridge JM, Halliwell B. Iron toxicity and oxygen radicals. Baillieres Clin Haematol 1989;2:195–256.
[5] Meshnick SR, Thomas A, Ranz A, Xu CM, Pan HZ. Artemisinin (qinghaosu): the role of intracellular hemin in its mechanism of antimalarial action. Mol Biochem Parasitol 1991;49:181–9.
[6] Posner GH, Oh CH, Wang D, Gerena L, Milhous WK, Meshnick SR, et al. Mechanism-based design, synthesis, and in vitro antimalarial testing of new 4-methylated trioxanes structurally related to artemisinin: the importance of a carbon-centered radical for antimalarial activity. J Med Chem 1994;37:1256–8.
[7] Eckstein-Ludwig U, Webb RJ, Van Goethem ID, East JM, Lee AG, Kimura M, et al. Artemisinins target the SERCA of *Plasmodium falciparum*. Nature 2003;424:957–61.
[8] Stocks PA, Bray PG, Barton VE, Al-Helal M, Jones M, Araujo NC, et al. Evidence for a common non-heme chelatable-iron-dependent activation mechanism for semisynthetic and synthetic endoperoxide antimalarial drugs. Angew Chem Int Ed Engl 2007;46:6278–83.
[9] Meshnick SR, Taylor TE, Kamchonwongpaisan S. Artemisinin and the antimalarial endoperoxides: from herbal remedy to targeted chemotherapy. Microbiol Rev 1996;60:301–15.
[10] Robert A, Meunier B. Is alkylation the main mechanism of action of the antimalarial drug artemisinin? Chem Soc Rev 1998;27:273–9.
[11] Cazelles J, Robert A, Meunier B. Alkylating capacity and reaction products of antimalarial trioxanes after activation by a heme model. J Org Chem 2002;67:609–19.
[12] Robert A, Coppel Y, Meunier B. Alkylation of heme by the antimalarial drug artemisinin. Chem Commun (Camb) 2002;5:414–5.
[13] Creek DJ, Charman WN, Chiu FC, Prankerd RJ, Dong Y, Vennerstrom JL, et al. Relationship between antimalarial activity and heme alkylation for spiro- and dispiro-1,2,4-trioxolane antimalarials. Antimicrob Agents Chemother 2008;52:1291–6.
[14] Loup C, Lelievre J, Benoit-Vical F, Meunier B. Trioxaquines and heme-artemisinin adducts inhibit the in vitro formation of hemozoin better than chloroquine. Antimicrob Agents Chemother 2007;51:3768–70.
[15] Robert A, Benoit-Vical F, Claparols C, Meunier B. The antimalarial drug artemisinin alkylates heme in infected mice. Proc Natl Acad Sci USA 2005;102:13676–80.
[16] Goldberg DE, Slater AF, Cerami A, Henderson GB. Hemoglobin degradation in the malaria parasite *Plasmodium falciparum*: an ordered process in a unique organelle. Proc Natl Acad Sci USA 1990;87:2931–5.
[17] Meshnick SR. Artemisinin: mechanisms of action, resistance and toxicity. Int J Parasitol 2002;32:1655–60.
[18] Maeno Y, Toyoshima T, Fujioka H, Ito Y, Meshnick SR, Benakis A, et al. Morphologic effects of artemisinin in *Plasmodium falciparum*. Am J Trop Med Hyg 1993;49:485–91.
[19] Del Pilar Crespo M, Avery TD, Hanssen E, Fox E, Robinson TV, Valente P, et al. Artemisinin and a series of novel endoperoxide antimalarials exert early effects on digestive vacuole morphology. Antimicrob Agents Chemother 2008;52:98–109.
[20] O'Neill PM, Posner GH. A medicinal chemistry perspective on artemisinin and related endoperoxides. J Med Chem 2004;47:2945–64.
[21] Haynes RK, Chan WC, Lung CM, Uhlemann AC, Eckstein U, Taramelli D, et al. The Fe^{2+}-mediated decomposition, PfATP6 binding, and antimalarial activities of artemisone and other artemisinins: the unlikelihood of C-centered radicals as bioactive intermediates. ChemMedChem 2007;2:1480–97.
[22] Bhisutthibhan J, Pan XQ, Hossler PA, Walker DJ, Yowell CA, Carlton J, et al. The *Plasmodium falciparum* translationally controlled tumor protein homolog and its reaction with the antimalarial drug artemisinin. J Biol Chem 1998;273:16192–8.
[23] Jambou R, Legrand E, Niang M, Khim N, Lim P, Volney B, et al. Resistance of *Plasmodium falciparum* field isolates to in vitro artemether and point mutations of the SERCA-type PfATPase6. Lancet 2005;366:1960–3.
[24] Krungkrai SR, Yuthavong Y. The antimalarial action on *Plasmodium falciparum* of qinghaosu and artesunate in combination with agents which modulate oxidant stress. Trans R Soc Trop Med Hyg 1987;81:710–4.
[25] Wei N, Sadrzadeh SM. Enhancement of hemin-induced membrane damage by artemisinin. Biochem Pharmacol 1994;48:737–41.
[26] Berman PA, Adams PA. Artemisinin enhances heme-catalysed oxidation of lipid membranes. Free Radic Biol Med 1997;22:1283–8.
[27] Disbrow GL, Baege AC, Kierpiec KA, Yuan H, Centeno JA, Thibodeaux CA, et al. Dihydroartemisinin is cytotoxic to papillomavirus-expressing epithelial cells in vitro and in vivo. Cancer Res 2005;65:10854–61.
[28] Li W, Mo W, Shen D, Sun L, Wang J, Lu S, et al. Yeast model uncovers dual roles of mitochondria in action of artemisinin. PLoS Genet 2005;1:e36.
[29] Lambros C, Vanderberg JP. Synchronization of *Plasmodium falciparum* erythrocytic stages in culture. J Parasitol 1979;65:418–20.
[30] Posner GH, Oh CH, Gerena L, Milhous WK. Extraordinarily potent antimalarial compounds: new, structurally simple, easily synthesized, tricyclic 1,2,4-trioxanes. J Med Chem 1992;35:2459–67.
[31] Posner GH, Paik IH, Sur S, McRiner AJ, Borstnik K, Xie S, et al. Orally active, antimalarial, anticancer, artemisinin-derived trioxane dimers with high stability and efficacy. J Med Chem 2003;46:1060–5.
[32] Bennett TN, Paguio M, Gligorijevic B, Seudieu C, Kosar AD, Davidson E, et al. Novel, rapid, and inexpensive cell-based quantification of antimalarial drug efficacy. Antimicrob Agents Chemother 2004;48:1807–10.
[33] Smilkstein M, Sriwilaijaroen N, Kelly JX, Wilairat P, Riscoe M. Simple and inexpensive fluorescence-based technique

for high-throughput antimalarial drug screening. Antimicrob Agents Chemother 2004;48:1803–6.
[34] Saliba KJ, Folb PI, Smith PJ. Role for the *Plasmodium falciparum* digestive vacuole in chloroquine resistance. Biochem Pharmacol 1998;56:313–20.
[35] Saliba KJ, Allen RJ, Zissis S, Bray PG, Ward SA, Kirk K. Acidification of the malaria parasite's digestive vacuole by a H+-ATPase and a H+-pyrophosphatase. J Biol Chem 2003;278:5605–12.
[36] Kuehl RO. Design of experiments: statistical principles of research design and analysis. Pacific Grove, CA: Duxbury Thomson Learning; 2000.
[37] Jackson KE, Klonis N, Ferguson DJ, Adisa A, Dogovski C, Tilley L. Food vacuole-associated lipid bodies and heterogeneous lipid environments in the malaria parasite, *Plasmodium falciparum*. Mol Microbiol 2004;54:109–22.
[38] Pisciotta JM, Coppens I, Tripathi AK, Scholl PF, Shuman J, Bajad S, et al. The role of neutral lipid nanospheres in *Plasmodium falciparum* haem crystallization. Biochem J 2007;402:197–204.
[39] Hammond EW. Chromatography for the analysis of lipids. Boca Raton, FL: CRC Press; 1993.
[40] Janoszka B, Wielkoszynski T, Tyrpien K, Dobosz C, Bodzek D. Effect of steroid hormones on results from the determination of oxycholesterol by TLC. Acta Chromatogr 2003;13:95–101.
[41] Vyas N, Avery BA, Avery MA, Wyandt CM. Carrier-mediated partitioning of artemisinin into *Plasmodium falciparum*-infected erythrocytes. Antimicrob Agents Chemother 2002;46:105–9.
[42] White N. Antimalarial drug resistance and combination chemotherapy. Philos Trans R Soc Lond B Biol Sci 1999;354:739–49.
[43] White NJ. Qinghaosu (artemisinin): the price of success. Science 2008;320:330–4.
[44] Palacpac NM, Hiramine Y, Mi-ichi F, Torii M, Kita K, Hiramatsu R, et al. Developmental-stage-specific triacylglycerol biosynthesis, degradation and trafficking as lipid bodies in *Plasmodium falciparum*-infected erythrocytes. J Cell Sci 2004;117:1469–80.
[45] Greenspan P, Fowler SD. Spectrofluorometric studies of the lipid probe, nile red. J Lipid Res 1985;26:781–9.
[46] Uhlemann AC, Wittlin S, Matile H, Bustamante LY, Krishna S. Mechanism of antimalarial action of the synthetic trioxolane RBX11160 (OZ277). Antimicrob Agents Chemother 2007;51:667–72.
[47] Posner GH, Chang W, Hess L, Woodard L, Sinishtaj S, Usera. et al. Malaria-infected mice are cured by oral administration of new artemisinin derivatives. J Med Chem 2008;51:1035–42.
[48] Meshnick SR, Yang YZ, Lima V, Kuypers F, Kamchonwongpaisan S, Yuthavong Y. Iron-dependent free radical generation from the antimalarial agent artemisinin (qinghaosu). Antimicrob Agents Chemother 1993;37:1108–14.
[49] Pap EH, Drummen GP, Winter VJ, Kooij TW, Rijken P, Wirtz KW, et al. Ratio-fluorescence microscopy of lipid oxidation in living cells using C11-BODIPY(581/591). FEBS Lett 1999;453:278–82.
[50] Karle JM, Karle IL. Crystal structure of (−)-mefloquine hydrochloride reveals consistency of configuration with biological activity. Antimicrob Agents Chemother 2002;46:1529–34.
[51] Vielemeyer O, McIntosh MT, Joiner KA, Coppens I. Neutral lipid synthesis and storage in the intraerythrocytic stages of *Plasmodium falciparum*. Mol Biochem Parasitol 2004;135:197–209.
[52] Murphy DJ. The biogenesis and functions of lipid bodies in animals, plants and microorganisms. Prog Lipid Res 2001;40:325–438.
[53] Coppens I, Vielemeyer O. Insights into unique physiological features of neutral lipids in Apicomplexa: from storage to potential mediation in parasite metabolic activities. Int J Parasitol 2005;35:597–615.
[54] Elliott DA, McIntosh MT, Hosgood 3rd HD, Chen S, Zhang G, Baevova P, et al. Four distinct pathways of hemoglobin uptake in the malaria parasite *Plasmodium falciparum*. Proc Natl Acad Sci USA 2008;105:2463–8.
[55] Gligorijevic B, Purdy K, Elliott D, Cooper RA, Roepe PD. Stage independent chloroquine resistance and chloroquine toxicity revealed via spinning disk confocal microscopy. Mol Biochem Parasitol 2008;159:7–23.
[56] Mercer AE, Maggs JL, Sun XM, Cohen GM, Chadwick J, O'Neill PM, et al. Evidence for the involvement of carbon-centered radicals in the induction of apoptotic cell death by artemisinin compounds. J Biol Chem 2007;282:9372–82.
[57] Creek DJ, Chiu FC, Prankerd RJ, Charman SA, Charman WN. Kinetics of iron-mediated artemisinin degradation: effect of solvent composition and iron salt. J Pharm Sci 2005;94:1820–9.
[58] Lytton J, Westlin M, Hanley MR. Thapsigargin inhibits the sarcoplasmic or endoplasmic reticulum Ca-ATPase family of calcium pumps. J Biol Chem 1991;266:17067–71.
[59] Kumaratilake LM, Robinson BS, Ferrante A, Poulos A. Antimalarial properties of n-3 and n-6 polyunsaturated fatty acids: in vitro effects on *Plasmodium falciparum* and in vivo effects on *P. berghei*. J Clin Invest 1992;89:961–7.
[60] Bozdech Z, Llinas M, Pulliam BL, Wong ED, Zhu J, DeRisi JL. The transcriptome of the intraerythrocytic developmental cycle of *Plasmodium falciparum*. PLoS Biol 2003;1:E5.
[61] Nawabi P, Lykidis A, Ji D, Haldar K. Neutral-lipid analysis reveals elevation of acylglycerols and lack of cholesterol esters in *Plasmodium falciparum*-infected erythrocytes. Eukaryot Cell 2003;2:1128–31.
[62] Carpenter KL. Good COP, bad COP: an unsolved murder. Are dietary cholesterol oxidation products guilty of atherogenicity? Br J Nutr 2002;88:335–8.
[63] Valenzuela A, Sanhueza J, Nieto S. Cholesterol oxidation: health hazard and the role of antioxidants in prevention. Biol Res 2003;36:291–302.
[64] Bjorkhem I, Diczfalusy U. Oxysterols: friends, foes, or just fellow passengers? Arterioscler Thromb Vasc Biol 2002;22:734–42.
[65] Lauer S, VanWye J, Harrison T, McManus H, Samuel BU, Hiller NL, et al. Vacuolar uptake of host components, and a role for cholesterol and sphingomyelin in malarial infection. EMBO J 2000;19:3556–64.
[66] Schwarzer E, Kuhn H, Valente E, Arese P. Malaria-parasitized erythrocytes and hemozoin nonenzymatically generate large amounts of hydroxy fatty acids that inhibit monocyte functions. Blood 2003;101:722–8.
[67] Huang XJ, Li CT, Zhang WP, Lu YB, Fang SH, Wei EQ. Dihydroartemisinin potentiates the cytotoxic effect of temozolomide in rat C6 glioma cells. Pharmacology 2008;82:1–9.
[68] El-Bassiouni EA, Helmy MH, Saad EI, El-Nabi Kamel MA, Abdel-Meguid E, Hussein HS. Modulation of the antioxidant defence in different developmental stages of *Schistosoma mansoni* by praziquantel and artemether. Br J Biomed Sci 2007;64:168–74.